Geophysical Research Letters

Amagmatic Subduction Produced by Mantle Serpentinization and Oceanic Crust Delamination

Jianfeng Yang[1,2] [iD], Gang Lu[1,3], Tong Liu[1] [iD], Yang Li[1,3] [iD], Kun Wang[1], Xinxin Wang[1], Baolu Sun[1,3], Manuele Faccenda[2] [iD], and Liang Zhao[1,3] [iD]

[1]State Key Laboratory of Lithospheric Evolution, Institute of Geology and Geophysics, Chinese Academy of Sciences, Beijing, China, [2]Dipartimento di Geoscienze, Università di Padova, Padua, Italy, [3]Institute of Earth Science, University of Chinese Academy of Sciences, Beijing, China

Abstract Recycling of oceanic lithosphere and serpentinized peridotites into the mantle leads to dehydration melting and volcanic arcs. However, the mechanism of the occurrence of long-term volcanic gap in subduction zones remains poorly understood. Two-dimensional thermomechanical numerical models focusing on resisting the transport of the major hosts of hydrous minerals to mantle depths, show that thin oceanic crust together with rheologically weak and buoyant serpentinized mantle could result in hydrated lithologies piling up in the accretionary wedge and no or sparse occurrence of arc magmatism. This scenario may occur during subduction of oceanic lithosphere formed at (ultra)slow-spreading margins characterized by thin crust and extensive mantle serpentinization, which is a plausible explanation for the "arc gaps" in the Alps and southern Tibet.

Plain Language Summary Volcanic arcs in subduction zones are widespread and are mainly attributed to slab dehydration and subsequent mantle hydrous melting. However, the magmatic history of the Alps and southern Tibet is characterized by two periods of "arc gap" (i.e., no volcanism) that lasted for 40–50 Myr and 10–30 Myr, respectively, with no or only very sparse magmatism and simultaneous exhumation of serpentinized mantle slivers. Our numerical models indicate that thin oceanic crust, such as that formed at (ultra)slow-spreading centers, together with an extensively serpentinized lithosphere facilitates the removal of the subducting crust at shallow depths resulting in limited arc magmatism.

1. Introduction

The occurrence of arc magmatism is a common feature in subduction zones, which is characterized by typical calc-alkaline magmatism and is mainly attributed to the continuous input of slab-derived fluids (Grove et al., 2012; Hirschmann, 2006; Peacock, 1990; Wallace, 2005; Zheng et al., 2016), although decompression melting may also occur (Sisson & Bronto, 1998). However, arc magmatism is not necessarily active throughout the history of a subduction zone. Two such examples are the periods of magmatic hiatus, or "arc gaps," inferred during the subduction of the Piemonte-Ligurian ocean in the Alps from ~100–50 Ma (McCarthy et al., 2018) and the Neo-Tethys Ocean in southern Tibet from ~145–120 Ma (Xiong et al., 2016). Such gaps in magmatic activity put forward an outstanding question: What controls volcanic arc gaps during subduction?

Exposed voluminous rift-related serpentinites and paucity of basalts and gabbros in ophiolites within the Alpine domain (Hattori & Guillot, 2007; Schaltegger et al., 2002), which are remnants of the magma-poor Piemonte-Ligurian Tethys (Manatschal & Müntener, 2009), are similar to present-day ultraslow-spreading ridges. Similar geological features have also been observed in Yarlung Zangbo ophiolites, in southern Tibet (Liu et al., 2014; Maffione et al., 2015). The slow- to ultraslow-spreading ridges, including the Mid-Atlantic Ridge (e.g., Kelley et al., 2001), Southwest Indian Ridge (e.g., Cannat et al., 2010), Gakkel Ridge in the Arctic Ocean (e.g., Lutz et al., 2018), and Mid-Cayman Spreading Center in central America (e.g., Grevemeyer et al., 2018), have very low magma supply with no or sporadic volcanic activity (e.g., Dick, 1989), and thus thin oceanic crust. Seismic and gravity studies of these slow-spreading ridges indeed reveal anomalously thinner oceanic crust and the presence of oceanic core complexes along detachment faults. In such an environment, seawater may interact with peridotite exposed at the flank of the ridge axis or infiltrate into the underlying mantle along detachment faults reaching depths of 2 to 15 km (Cannat

et al., 2010; Lutz et al., 2018) resulting in the formation of abyssal serpentinites. Serpentinites are rheologically weak and are buoyant and water-rich when compared to dry peridotite. It has been demonstrated that subduction of abyssal serpentinites formed at (ultra)slow-spreading ridges likely influences subduction zone processes especially hydrous melting (Gerya et al., 2002; Guillot et al., 2015; Hirth & Guillot, 2013).

The cause of the arc gap in the Alps and the southern Tibet is conventionally attributed to forearc hyperextension and/or trench migration (Maffione et al., 2015; Xiong et al., 2016), slab breakoff (Butler & Beaumont, 2017), and flat-slab subduction (Bergomi et al., 2015; Coulon et al., 1986; Hao et al., 2019; Kapp et al., 2005; Zhang et al., 2019). First, forearc hyperextension induced by trench migration is unlikely to prevent dehydration melting if subduction of hydrated oceanic lithosphere is continuous as it appears to be the case during the Cretaceous in southern Tibet. Second, slab breakoff, although hindering hydrous melting, will facilitate decompression melting of the upwelling asthenosphere (e.g., Freeburn et al., 2017). Finally, flat-slab geometries are generally attributed to strong mantle wedge suction forces (van Hunen et al., 2004), to the subduction of thick oceanic crust and/or harzburgite/serpentinized layer or a young thermally buoyant slab (Huangfu et al., 2016; Park & Rye, 2019). It has been suggested that this would form a cold forearc during flat-slab subduction (Dumitru et al., 1991), which leads to waning of magmatism (Gutscher et al., 2000). For instance, the recognized volcanic gaps in Andes are coincident with the flat-slab segments. However, only ~10% of all subduction zones have a shallow subducting angle. Moreover, four of the 10 known flat subduction zones still result in arc magmatism, and eight of them are linked to the occurrence of adakites (Gutscher et al., 2000). Furthermore, flat-slab subduction is usually transient and probably only lasts for <10 Ma (McCarthy et al., 2018; Ramos & Folguera, 2009), which is not consistent with the long-term (>10 Ma) magmatic hiatus in the Alps and southern Tibet. Thus, interruptions in arc magmatism are difficult to explain the arc gap when fluid input into the mantle wedge is continuous. An alternative explanation is that arc gaps are associated with a "dry" subducting plate (McCarthy et al., 2018).

Previous numerical models have shown that the presence of partially serpentinized mantle could decouple the oceanic crust (a process known as crustal "delamination") from the subducting plate, with the crust that later piles up within the accretionary wedge (Ruh et al., 2015; Vogt & Gerya, 2014). If this is the case, it would decrease the efficiency of water transportation to the mantle if crustal delamination occurs at shallow depths reducing melt production. Another mechanism that allows for water infiltration and mantle serpentinization down to 5–20 km below the Moho is by normal faulting associated with slab bending prior to subduction (Faccenda et al., 2009; Ivandic et al., 2008). In the last two decades, it has become clear that this slab hydration mechanism can substantially affect the efficiency of water transported into the subarc mantle (Faccenda, 2014). Here, we use petrological-thermomechanical numerical models to investigate the influence of these two different types of serpentinized mantle and oceanic crust hydration on the arc magmatic production. We find that subducting plates with a thin oceanic crust together with a highly serpentinized mantle could result in no or sparse arc magmatism, and it is thus a potential explanation for the "arc gaps" in the Alps and southern Tibet.

2. Methods

The two-dimensional petrological-thermomechanical numerical code I2VIS (Gerya & Yuen, 2003) is based on a finite difference method using marker-in-cell technique, which solves the incompressible flow using the Boussinesq approximation. Readers may refer to Gerya and Yuen (2003) and supporting information for a detailed description of the employed numerical strategy.

The model domain is 1,500 km × 310 km along *x-y* coordinates, and includes a 900 km wide oceanic plate (Figure S1). We employ 751 × 311 uniformly spaced nodes which result in a resolution of 2 km × 1 km in *x* and *y* directions, respectively (resolution test with 1 km × 0.5 km node spacing generates a similar result). A weak zone is assigned to facilitate subduction initiation. The overriding plate has a 20-km thick continental crust representing an Alps-like extended and thinned continental margin (Manatschal & Müntener, 2009). Within the subducting plate we vary the thicknesses of the oceanic crust and the extent of mantle serpentinization.

The mechanical boundary conditions are everywhere free slip except the bottom boundary which is permeable. A 10-km low viscosity "sticky" air at the top boundary is implemented to mimic free surface for the finite difference method (Crameri et al., 2012; Gerya, 2019). A constant convergence rate of 2.5 cm/yr is

applied at $x = 500$ km on the subducting plate. The initial temperature is given by a 50 Myr-old half-space cooling profile for the oceanic plate and the geotherm for the continental lithosphere is linear in the crust and mantle lithosphere with a Moho temperature of 400 °C at the Moho and a temperature of 1300 °C at the base of lithosphere. The temperature gradient in the crust is consistent with the metamorphic P-T conditions in the Alps (Müntener et al., 2000). The adiabatic thermal gradient is set to 0.5 K/km in the asthenospheric mantle. Thermal boundary conditions are isothermal at the top (0 °C) and bottom (1450 °C) boundaries, and zero heat flux at the side boundaries.

The water content of the hydrated rocks and the dehydration reactions are computed with PERPLE_X (Connolly, 2005). In situ maximum water content of each rock phase is calculated as a function of pressure and temperature from a precomputed look-up table. The stability of serpentine (containing 12–13 wt.% of water) is taken from Schmidt and Poli (1998). When the serpentine is beyond the stabilization by P-T conditions, it will dehydrate and turn to wet mantle. The water in excess will be stored on newly generated markers which migrate upward until they are absorbed by unsaturated markers (Faccenda et al., 2012; Yang & Faccenda, 2020). The initial water content for the oceanic crust and sediments are assumed to be saturated yielding an upper-bound estimation of magma genesis. The water content in the partially serpentinized mantle beneath the Moho depends on the degree of serpentinization ω ($\omega = 30\%$ corresponds to ~2 wt.% of water), and its effective density is

$$\rho_{\text{serp}}^{\text{eff}} = (1 - \omega)\rho_{\text{dry}} + \omega\rho_{\text{serp}} \tag{1}$$

where $\rho_{\text{serp}}(= 2{,}950 \text{ kg/m}^3)$, ρ_{dry} are densities of serpentinized and dry mantle, respectively.

The partial melting of sediments, oceanic crust, and peridotite, together with melt extraction processes are also modeled (Yang & Faccenda, 2020). To account for partial melting of the sediment, the metamorphosed oceanic crust and the peridotite, a linear parameterization of melt fraction (equations 2–4) between solidus and liquidus is used. The peridotite solidus is adjusted for the extent of hydration following Litasov et al. (2013).

$$M_0 = 0 \qquad\qquad \text{when } T \leq T_{\text{solidus}} \tag{2}$$

$$M_0 = \frac{T - T_{\text{solidus}}}{T_{\text{liquidus}} - T_{\text{solidus}}} \quad \text{when } T_{\text{solidus}} < T < T_{\text{liquidus}} \tag{3}$$

$$M_0 = 1 \qquad\qquad \text{when } T \geq T_{\text{sliquidus}} \tag{4}$$

We assume that melt is extracted when the melt fraction exceeds a critical value ($M_{\text{crit}}=0.05$). The amount of melt M presents at any time in each particle considered the amount that has been extracted during earlier events (e.g., Yang et al., 2018). The extracted melt moves instantaneously upward to generate the new crust (20% as volcanic rocks erupted at the surface and the remaining 80% as plutons emplaced at larger depths where crustal dilation is the largest).

The goal of this study is to identify scenarios leading to amagmatic subduction zones. We focus on the influence of abyssal and slab bending-related serpentinites on oceanic crust delamination. For abyssal serpentinites, both the degree of serpentinization (0–40%) and the thickness of the serpentinized layer are varied. Similarly, the maximum depth of serpentinization (5–20 km) and its extent (10–30%) are varied for serpentinites forming along bending-related normal faults (a full list of the models is given in the supporting information).

3. Experimental Results

To investigate the influence of hydrated oceanic crust and serpentinized mantle on the genesis of arc magmatism, we have chosen three end-member model setups that are representative of the upper oceanic lithosphere formed at normal- and slow-spreading ridges: (1) an oceanic crust with a normal thickness but without serpentine layer; (2) an oceanic crust with normal thickness together with a slab bending-induced serpentinized mantle; and (3) an abyssal serpentinized mantle underlying a thin oceanic crust (Figure 1). We find that the first two models with normal oceanic crust can carry water to the mantle depths that
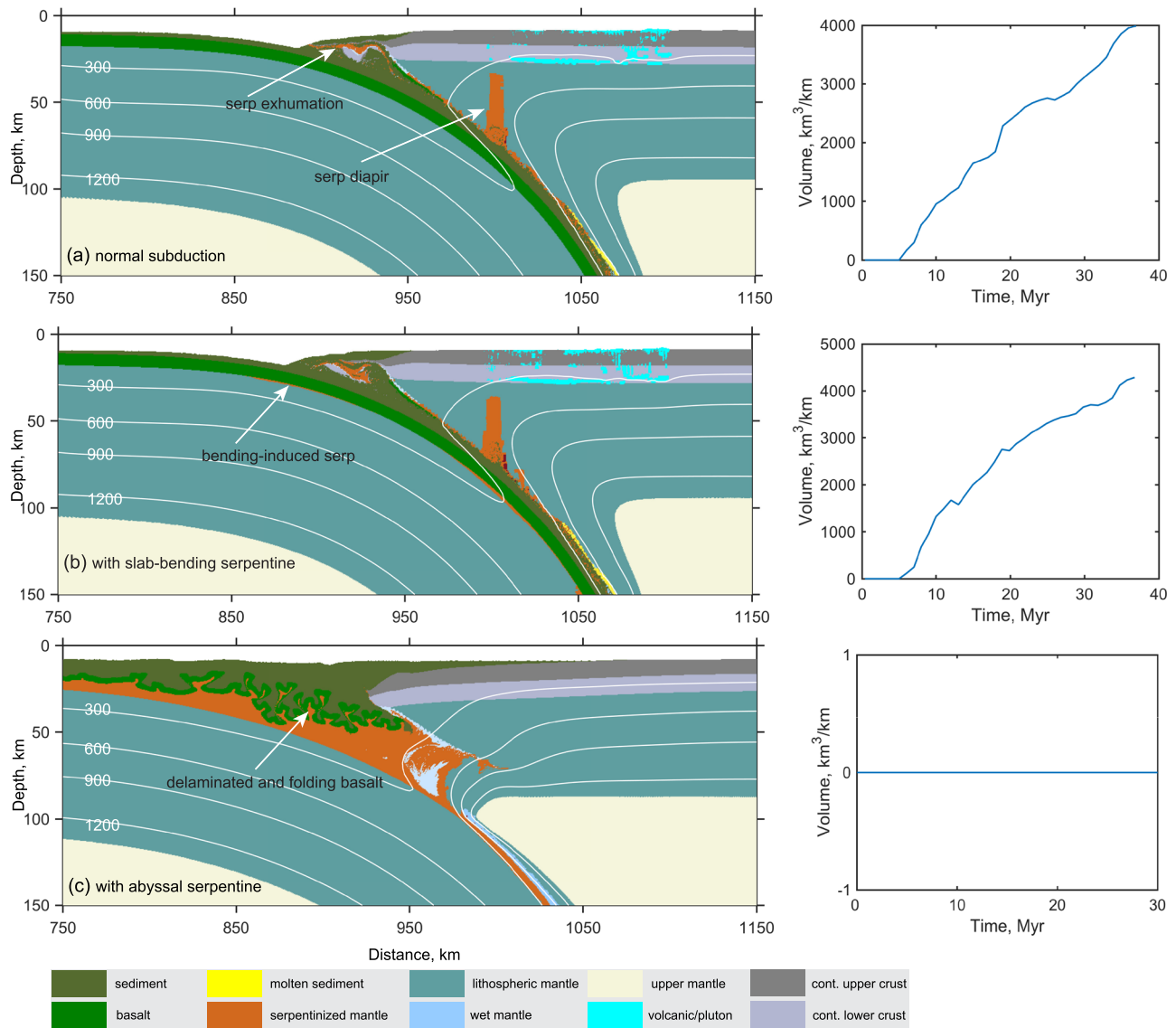
Figure 1. Model results. (a) Normal subduction with 7-km oceanic crust. The left panel shows composition field overlaid by isotherms (white lines) in °C. The right panel shows (reference) evolution of total magmatic volume over time. (b) Subduction with 7-km thick oceanic crust and with slab-bending serpentinite. The evolution of magmatic volume is similar as Model . (c) Subduction 2-km thick oceanic crust and with 5-km thick abyssal serpentinite. Note that the oceanic crust is stacking at the trench instead of subducting downward such that no magmatism occurs.

facilitate arc magmatism, while the last situation results in an amagmatic arc. The subducting plate dehydrates at ~80 km depth forming buoyant serpentinized diapirs. The subducted sediments are molten at ~90 km forming early magmatism. Below the overriding plate, serpentine breaks down at ~150 km inducing hydrous flux melting upon the release of fluids into the hot mantle wedge region and arc volcanism at the surface. The (ultra)slow-spreading ridges are characterized by episodic magmatism resulting in a very thin oceanic crust overlying a serpentinized lithospheric mantle. The serpentinized layer decouples the overlying basalt from the underlying subducting plate. As a result, in these models the subduction channel is filled with serpentinites, while all the basalts are peeled off from the slab and piled up to the accretionary wedge (Figure 1c). In cold slabs the water stored in the remaining serpentinized layer is partially released at intermediate depths and, upon formation of dense hydrous magnesium silicate (DHMS) phases (Iwamori, 2004), subsequently subducted to greater depths (Yang & Faccenda, 2020). Obviously, no dehydration event from the delaminated oceanic crust or sediment can further supply
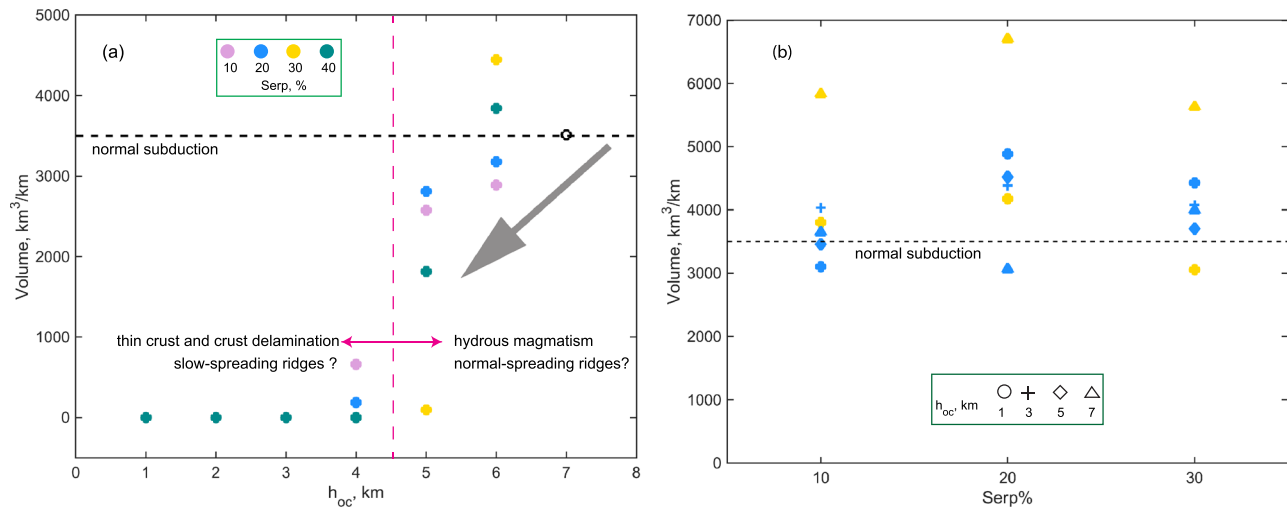
Figure 2. (a) Oceanic crustal thickness versus magmatic volume (at ~28 Myr) for different extents of abyssal serpentinization (color indicated). Note the sharp transition from magmatic arc to amagmatic arc at 4–5 km thick oceanic crust. (b) Different slab-bending induced serpentinization extents versus magmatic volume. The blue and yellow colors in (b) indicate serpentinization at strain of 0.1 and 0.01, respectively. The dashed line indicates normal magmatic volume at reference model.

mantle melting. As we find that the occurrence of arc amagmatism primarily depends on the detachment of the oceanic crust from the underlying mantle, in the following we describe our model results as a function of oceanic crust delamination.

3.1. Abyssal Serpentinite

To investigate the interaction between the crust and serpentinized upper mantle on arc magma production, we systematically vary the thickness and degree of serpentinization of these two layers. The total thickness of the crust and serpentinized mantle is held constant at 7 km (except the models in Figure 3 where we systematically vary the thickness of crustal and serpentinized layers). The volume of arc magmatism decreases with a thinner oceanic crust, while it generally increases with a larger degree of serpentinization. When serpentinization is more extensive (40%), a thick oceanic crust can be partially or fully peeled off from the slab, which decreases the amount of water transported deeper into the mantle. In this latter case only a small amount of subducted serpentinite breaks down and triggers melting at ~100 km. There is almost no arc magmatism when the oceanic crust is thinner than 4 km (Figure 2).

3.2. Slab Bending-Related Serpentinite

As the extent of serpentinization within bending-related fractures is relatively uncertain, a moderate $\omega = 20\%$ is assumed. Bending-induced normal faulting extends from few to >20 km beneath the Moho (Cai et al., 2018; Ivandic et al., 2008). In our models, serpentinization occurs when the accumulated plastic strain along these normal faults exceeds a given threshold (Faccenda et al., 2008). For example, the thickness of a serpentinized layer with an accumulated plastic strain threshold of 0.1 (model *E01*) and of 0.01 (model *E001*) reaches, respectively, <5 and 10 km beneath the Moho. When the threshold of the accumulated plastic strain is higher (0.1; i.e., it is more difficult to form serpentinites) and the oceanic crust has a normal thickness (≥5 km), less serpentinites are produced so that the oceanic crust will not be scraped off and be coupled with the subducting slab as it descends beneath the arc. On the contrary, extensive serpentinization by brittle normal faults at the trench outer rise would enable partial delamination of the thin oceanic crust at different depths (Table S2). Serpentinization along bending-related normal faults is laterally discontinuous and the degree of serpentinization here has minor or no influence on the arc magmatism. However, the thickness of the serpentinized layer matters. The oceanic crust can hardly be fully delaminated at shallow depths and arc magmatism will always appear. The magmatic rock volume generally increases with the depth extent of bending-related serpentinization, that is, the deeper serpentinized layer (*E001*), the larger the magmatic volume. On the other hand, magmatism is decreasing with increasing thickness of the oceanic crust
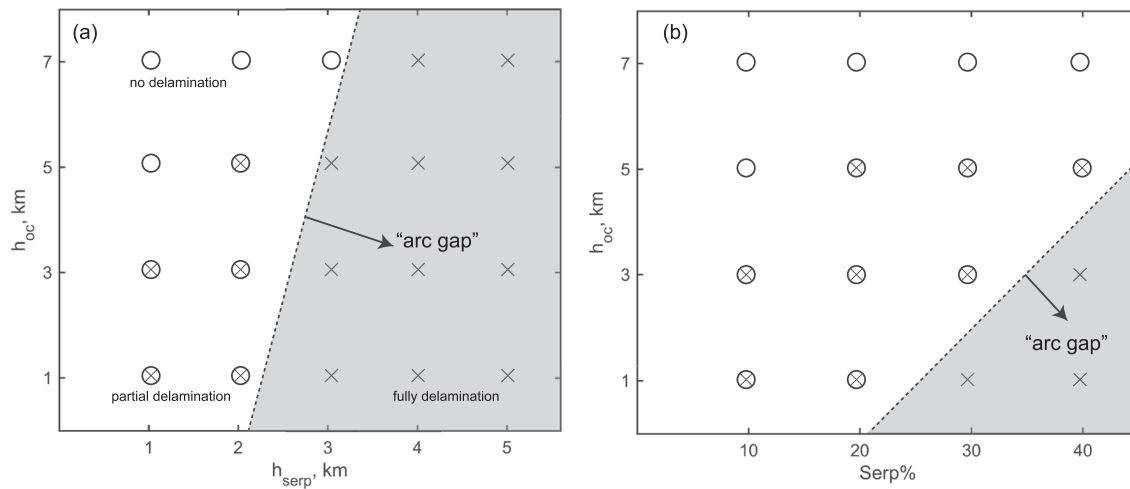
Figure 3. The occurrence of "arc gap" with abyssal serpentine for different model parameters (thickness of serpentine layer, oceanic crust, and serpentine extent). Arc magmatism regimes for various combinations of (a) serpentine thickness (with serpentine extent of 20%) and (b) serpentine extent (note that a constant thickness of 2 km serpentine was used here) versus oceanic crust thickness. A thin oceanic crust layer and a thick and/or a heavy serpentinized layer are more likely to result in "arc gap" scenario.

for *E01* models. This is because a thinner crust favors the heating and the dehydration of the sub-Moho serpentinized mantle.

4. Discussion

4.1. Thin Oceanic Crust and Abyssal Serpentinized Mantle Control Amagmatism

Our model results indicate that bending-related mantle serpentinization has limited influence on the generation of amagmatic arc conditions. The amagmatic scenario is largely controlled by the thickness of the oceanic crust and of the abyssal serpentinized mantle corresponding to those found at (ultra) slow-spreading ridges where thin oceanic crust and thick serpentinized peridotite contemporaneously develop. A $\geq$ 4-km-thick peridotite displaying a moderate degree ($\geq$20%) of serpentinization can readily result in full decoupling of the oceanic crust from the underlying mantle at shallow depths and amagmatic episodes (Figure 3). Ruh et al. (2015) also showed that a discontinuous serpentinization patch may not lead to oceanic crust delamination unless its wavelength is as large as 127.5 km. Our end-member model displays abyssal serpentinized mantle which is continuous (>127.5 km). A continuous slab-bending serpentinite layer in our models might also efficiently scrape off a thin oceanic crust (Figure S2c and S3c) which is consistent with Ruh et al. (2015).

A thicker serpentinized layer or a higher modal abundance of serpentine promotes the detachment of the oceanic crust, whereas other factors, such as the weak zone in the model setup and the strength of the oceanic crust, might also affect this process. Additional model tests show that the width and initial dip angle of weak zone have almost no influence on the dynamics (Figure S4). A very low friction coefficient or cohesion (thus low yield stress) is required for the occurrence of oceanic crust delamination. Such friction coefficient is much lower than that of dry rocks measured in laboratory experiments (usually 0.6–0.8), and it might be representative for the rocks along oceanic detachment faults formed at (ultra) slow-spreading ridges or present along subduction channels (Sobolev & Brown, 2019) where increased pore pressure significantly decreases the effective friction coefficient. In contrast, a much larger friction angle thus larger yield stress in pristine and dry oceanic crust that cannot be resisted by buoyancy stresses (Figure S5), such as that characterizing the oceanic lithosphere formed at intermediate- to fast-spreading ridges, would require an unrealistically thick and heavily serpentinized layer to induce crust delamination. This suggests that in the latter case the crustal delamination mechanism proposed here cannot explain arc gap episodes.
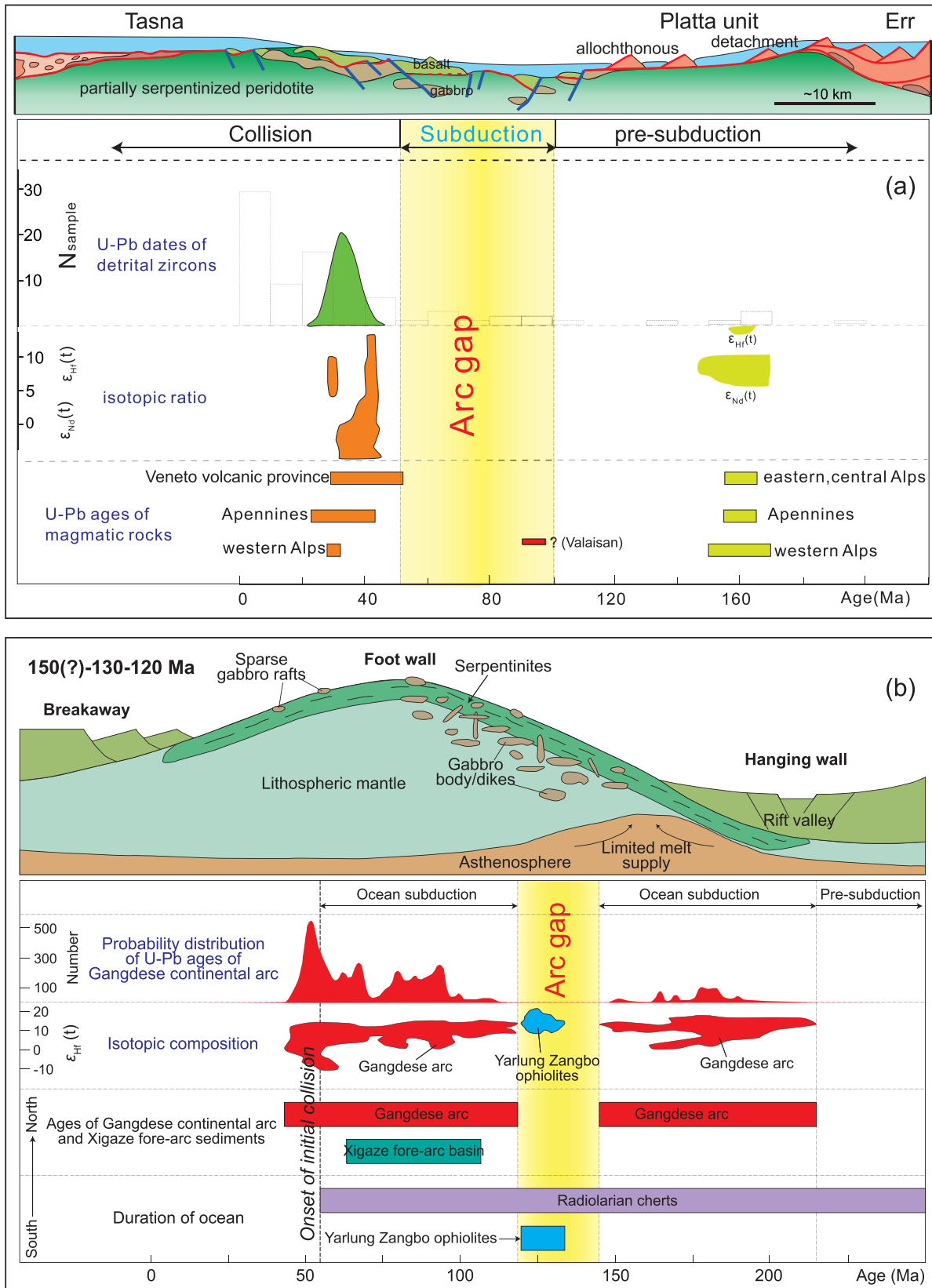
Figure 4. (a) Palinspastic reconstruction based on Schaltegger et al. (2002) and Manatschal and Müntener (2009), and igneous activity in the Alps modified from McCarthy et al. (2018). (b) Cartoon showing exhumation of the Purang peridotite massif after Liu et al. (2014) and igneous activity in southern Tibet.

4.2. Amagmatism in the Alps and Southern Tibet

Convergent plate margins are the sites where oceanic plate subducts and new continental crust forms via magmatic rock emplacement. However, the Alpine subduction zone, initiating at ~85–100 Ma, is a typical example of a magma-poor convergent margin (McCarthy & Müntener, 2015). Magmatic and metamorphic records during pre-subduction and collision in Alps have been widely observed (Figure 4, Ji et al., 2019; McCarthy et al., 2018). The magmatic arc gap lasting for more than 40 Ma (Figure 4a) during the Alpine subduction cannot be explained by the lack of preservation of volcanic and/or plutonic edifices (McCarthy et al., 2018). Field observations show that extensive serpentinized mantle peridotites intruded by gabbro bodies are the most significant geological features characteristic of the Alpine Jurassic Tethys (e.g., Lagabrielle & Cannat, 1990; Schaltegger et al., 2002). Geochemical study suggests that these serpentinites are hydrated abyssal peridotites (Hattori & Guillot, 2007). Our models show that a sporadically distributed oceanic crust overlying a weakly serpentinized mantle will be delaminated and emplaced at accretionary wedges. Thus, negligible water can be transported to mantle depths by subduction of crustal materials (McCarthy et al., 2018). Water may remain within the cold core of serpentinized slab mantle in hydrous phase A and other DHMS at higher pressures (Yang & Faccenda, 2020). Therefore, unlike arc magma in normal subduction zones, magmatism in this case is inhibited by accretion of the hydrated portions of the slab to the upper plate margin. The models indicate that arc gap or sparse magmatism occurs when the thickness of the serpentinized layer is larger than 3 km or the serpentinization extent is larger than 40% (Figure 3). Serpentinites are indeed extensive, up to 40% in some parts of Alps (Schwartz et al., 2001). Wide-angle seismic profiles in the present-day ocean-continent transition in the Alps suggests that serpentinized bodies probably extend down to 2–4 km (Dean et al., 2000) with the upper 2 km inferred to be pervasively serpentinized (~25–45%) peridotite (Chian et al., 1999).

Another "arc gap" occurred for a short period at ~145–120 Ma in the Gangdese arc in southern Tibet, China (Figure 4b). Ophiolites preserved along the Yarlung Zangbo suture zone (YZSZ) in southern Tibet have been interpreted as forming either in a suprasubduction zone (SSZ) or at a mid-ocean ridge (MOR). The Yarlung Zangbo ophiolites are characterized by thick (up to 10 km) highly serpentinized mantle peridotites (a proportion of >90% in the ophiolite) with sparsely distributed, very thin (<3 km) crustal rocks, which were linked to the oceanic lithosphere formed at modern slow-spreading ridges (Girardeau et al., 1985; Nicolas et al., 1981). For example, the Purang ophiolite from the western part of the YZSZ is composed of a ~800-km^2 mantle massif but scarce crustal units (Liu et al., 2014). Beside this, the Xigaze ophiolite from the central part of the YZSZ has variable crustal thickness, and its gabbro bodies occur only in a few massifs (Girardeau et al., 1985; Liu et al., 2016, 2018). Based on geological, structural, and paleomagnetic observations, recent studies have proposed that detachment faults may have dismembered the Yarlung Zangbo ophiolites, forming oceanic core complexes with thin and discontinuous crust and heavily serpentinized peridotites (Li et al., 2016; Liu et al., 2014; Maffione et al., 2015). Therefore, the crustal architecture of the Neo-Tethys Ocean is somewhat comparable to those from modern slow- and ultraslow-spreading ridges and the Alpine ophiolites. Numerous high-precision geochronological data shows that the Yarlung Zangbo ophiolites were formed over a short period of ~120–130 Ma (Liu et al., 2016, and references therein), which overlaps with the major arc gap for the Gangdese arc (Figure 4b). This inherently implies a genetic linkage between the crustal architecture of the Neo-Tethys Ocean in the Lower Cretaceous and the accretion of Gangdese arc. In other words, the thin and discontinuous crust and strong serpentinization of mantle peridotites may have prevented the transportation of water into the overlying wedge, resulting in the Gangdese arc gap at that time, as has been proposed in the Alps (McCarthy et al., 2018) and modeled in this study. Instead, the flat subduction, if hypothetically existed (Hao et al., 2019), could have been induced by the presence of a buoyant serpentinized layer produced in a (ultra)slow-spreading ridge, which would have further aided the magmatic hiatus.

5. Conclusions

Systematic numerical models are conducted to test the influence of serpentinites on the magmatism in subduction zones. We find that the existence of a rheologically weak and buoyant abyssal serpentinite layer could favor the delamination of an overlying thin oceanic crust, leading to no or sparse magmatism when

its thickness or degree of serpentinization is sufficiently large. The detachment of hydrated lithologies at shallow depths implies subduction of a "dry" subducting plate, which could be the mechanism explaining the "arc gap" observed in the Alps and southern Tibet. It is important to notice that the delamination of the oceanic crust may have profound influence on the recycling of volatiles species over geological time because the oceanic crust (including sediments) together with the serpentinized mantle is the major carrier of water and carbon into the mantle during subduction. As such, reduced volumes of volatiles would be recycled into the deep mantle where lithosphere created at (ultra)slow-spreading ridges is subducted.

References

Bergomi, M. A., Zanchetta, S., & Tunesi, A. (2015). The tertiary dike magmatism in the southern Alps: Geochronological data and geodynamic significance. *International Journal of Earth Sciences*, *104*, 449–473.

Butler, J. P., & Beaumont, C. (2017). Subduction zone decoupling/retreat modeling explains South Tibet (Xigaze) and other supra-subduction zone ophiolites and their UHP mineral phases. *Earth and Planetary Science Letters*, *463*, 101–117.

Cai, C., Wiens, D. A., Shen, W., & Eimer, M. (2018). Water input into the Mariana subduction zone estimated from ocean-bottom seismic data. *Nature*, *563*, 389.

Cannat, M., Fontaine, F., & Escartín, J. (2010). Serpentinization and associated hydrogen and methane fluxes at slow spreading ridges. In *Diversity of Hydrothermal Systems on Slow Spreading Ocean Ridges, Geophysical Monograph Series*. https://doi.org/10.1029/2008GM000760

Chian, D., Louden, K. E., Minshull, T. A., & Whitmarsh, R. B. (1999). Deep structure of the ocean-continent transition in the southern Iberia Abyssal Plain from seismic refraction profiles: Ocean Drilling Program (Legs 149 and 173) transect. *Journal of Geophysical Research*, *104*, 7443–7462.

Connolly, J. (2005). Computation of phase equilibria by linear programming: a tool for geodynamic modeling and its application to subduction zone decarbonation. *Earth and Planetary Science Letters*, *236*, 524–541.

Coulon, C., Maluski, H., Bollinger, C., & Wang, S. (1986). Mesozoic and Cenozoic volcanic rocks from central and southern Tibet: ^{39}Ar-^{40}Ar dating, petrological characteristics and geodynamical significance. *Earth and Planetary Science Letters*, *79*, 281–302. https://doi.org/10.1016/0012-821X(86)90186-X

Crameri, F., Schmeling, H., Golabek, G., Duretz, T., Orendt, R., Buiter, S., et al. (2012). A comparison of numerical surface topography calculations in geodynamic modelling: An evaluation of the 'sticky air' method. *Geophysical Journal International*, *189*, 38–54.

Dean, S., Minshull, T., Whitmarsh, R., & Louden, K. (2000). Deep structure of the ocean-continent transition in the southern Iberia Abyssal Plain from seismic refraction profiles: The IAM-9 transect at 40°20′N. *Journal of Geophysical Research*, *105*, 5859–5885.

Dick, H. (1989). Abyssal peridotites, very slow spreading ridges and ocean ridge magmatism. *Geological Society, London, Special Publications*, *42*, 71–105. https://doi.org/10.1144/GSL.SP.1989.042.01.06

Dumitru, T. A., Gans, P. B., Foster, D. A., & Miller, E. L. (1991). Refrigeration of the western Cordilleran lithosphere during Laramide shallow-angle subduction. *Geology*, *19*, 1145–1148. https://doi.org/10.1130/0091-7613(1991)019<1145:ROTWCL>2.3.CO;2

Faccenda, M. (2014). Water in the slab: A trilogy. *Tectonophysics*, *614*, 1–30. https://doi.org/10.1016/j.tecto.2013.12.020

Faccenda, M., Burlini, L., Gerya, T. V., & Mainprice, D. (2008). Fault-induced seismic anisotropy by hydration in subducting oceanic plates. *Nature*, *455*, 1097–1100. https://doi.org/10.1038/nature07376

Faccenda, M., Gerya, T. V., & Burlini, L. (2009). Deep slab hydration induced by bending-related variations in tectonic pressure. *Nature Geoscience*, *2*, 790–793. https://doi.org/10.1038/ngeo656

Faccenda, M., Gerya, T. V., Mancktelow, N. S., & Moresi, L. (2012). Fluid flow during slab unbending and dehydration: Implications for intermediate-depth seismicity, slab weakening and deep water recycling. *Geochemistry, Geophysics, Geosystems*, *13*(1).

Freeburn, R., Bouilhol, P., Maunder, B., Magni, V., & van Hunen, J. (2017). Numerical modelsof the magmatic processes induced by slab breakoff. *Earth and Planetary Science Letters*, *478*, 203–213.

Gerya, T. (2019). *Introduction to numerical geodynamic modelling*, (2nd ed.). Cambridge: Cambridge University Press.

Gerya, T. V., Stockhert, B., & Perchuk, A. L. (2002). Exhumation of high-pressure metamorphic rocks in a subduction channel: A numerical simulation. *Tectonics*, *21*(6), 6-1–6-19. https://doi.org/10.1029/2002tc001406

Gerya, T. V., & Yuen, D. A. (2003). Characteristics-based marker-in-cell method with conservative finite-differences schemes for modeling geological flows with strongly variable transport properties. *Physics of the Earth and Planetary Interiors*, *140*, 293–318. https://doi.org/10.1016/j.pepi.2003.09.006

Girardeau, J., Mercier, J. C. C., & Xibin, W. (1985). Petrology of the mafic rocks of the Xigaze ophiolite Tibet. *Contributions to Mineralogy and Petrology*, *90*, 309–321. https://doi.org/10.1029/TC004i003p00267

Grevemeyer, I., Ranero, C. R., & Ivandic, M. (2018). Structure of oceanic crust and serpentinization at subduction trenches. *Geosphere*, *14*, 395–418. https://doi.org/10.1130/GES01537.1

Grove, T. L., Till, C. B., & Krawczynski, M. J. (2012). The Role of H_2O in Subduction Zone Magmatism. *Annual Review of Earth and Planetary Sciences*, *40*, 413–439.

Guillot, S., Schwartz, S., Reynard, B., Agard, P., & Prigent, C. (2015). Tectonic significance of serpentinites. *Tectonophysics*, *646*, 1–19. https://doi.org/10.1016/j.tecto.2015.01.020

Gutscher, M.-A., Maury, R., Eissen, J.-P., & Bourdon, E. (2000). Can slab melting be caused by flat subduction? *Geology*, *28*, 535–538.

Hao, L.-L., Wang, Q., Zhang, C., Ou, Q., Yang, J.-H., Dan, W., & Jiang, Z.-Q. (2019). Oceanic plateau subduction during closure of the Bangong-Nujiang Tethyan Ocean: Insights from central Tibetan volcanic rocks. *GSA Bulletin*, *131*, 864–880. https://doi.org/10.1130/B32045.1

Hattori, K. H., & Guillot, S. (2007). Geochemical character of serpentinites associated with high-to ultrahigh-pressure metamorphic rocks in the Alps, Cuba, and the Himalayas: Recycling of elements in subduction zones. *Geochemistry, Geophysics, Geosystems*, *8*, Q09010. https://doi.org/10.1029/2007GC001594

Hirschmann, M. M. (2006). Water, melting, and the deep Earth H_2O cycle. *Annual Review of Earth and Planetary Sciences*, *34*, 629–653. https://doi.org/10.1146/annurev.earth.34.031405.125211

Hirth, G., & Guillot, S. (2013). Rheology and tectonic significance of serpentinite. *Elements*, *9*, 107–113. https://doi.org/10.2113/gselements.9.2.107

Huangfu, P., Wang, Y., Cawood, P. A., Li, Z.-H., Fan, W., & Gerya, T. V. (2016). Thermo-mechanical controls of flat subduction: Insights from numerical modeling. *Gondwana Research*, *40*, 170–183.

Ivandic, M., Grevemeyer, I., Berhorst, A., Flueh, E. R., & McIntosh, K. (2008). Impact of bending related faulting on the seismic properties of the incoming oceanic plate offshore of Nicaragua. *Journal of Geophysical Research*, *113*, B05410. https://doi.org/10.1029/2007JB005291

Iwamori, H. (2004). Phase relations of peridotites under H_2O-saturated conditions and ability of subducting plates for transportation of H_2O. *Earth and Planetary Science Letters*, *227*, 57–71. https://doi.org/10.1016/j.epsl.2004.08.013

Ji, W. Q., Malusà, M. G., Tiepolo, M., Langone, A., Zhao, L., & Wu, F. Y. (2019). Synchronous periadriatic magmatism in the Western and Central Alps in the absence of slab breakoff. *Terra Nova*. https://doi.org/10.1111/ter.12377

Kapp, P., Yin, A., Harrison, T. M., & Ding, L. (2005). Cretaceous-Tertiary shortening, basin development, and volcanism in central Tibet. *Geological Society of America Bulletin*, *117*, 865–878. https://doi.org/10.1130/B25595.1

Kelley, D. S., Karson, J. A., Blackman, D. K., FruÈh-Green, G. L., Butterfield, D. A., Lilley, M. D., et al. (2001). An off-axis hydrothermal vent field near the mid-Atlantic ridge at 30°N. *Nature*, *412*(6843), 145–149. https://doi.org/10.1038/35084000

Lagabrielle, Y., & Cannat, M. (1990). Alpine Jurassic ophiolites resemble the modern central Atlantic basement. *Geology*, *18*, 319–322. https://doi.org/10.1130/0091-7613(1990)018<0319:AJORTM>2.3.CO;2

Li, Y., Li, R., Dong, T., Yang, S., & Pei, L. (2016). Structure of the Baimarang massif in the Xigaze ophiolite, Yarlung Zangbo Suture Zone, southern Tibet, China. *Chinese Science Bulletin*, *61*, 2823–2833. https://doi.org/10.1360/N972016-00203

Litasov, K. D., Shatskiy, A., & Ohtani, E. (2013). *Earth's mantle melting in the presence of COH-bearing fluid*, (pp. 38–65). Wiley-Blackwell: Physics and Chemistry of Deep Earth.

Liu, C.-Z., Zhang, C., Yang, L.-Y., Zhang, L.-L., Ji, W.-Q., & Wu, F.-Y. (2014). Formation of gabbronorites in the Purang ophiolite (SW Tibet) through melting of hydrothermally altered mantle along a detachment fault. *Lithos*, *205*, 127–141. https://doi.org/10.1016/j.lithos.2014.06.019

Liu, T., Wu, F.-Y., Liu, C.-Z., Tribuzio, R., Ji, W.-B., Zhang, C., et al. (2018). Variably evolved gabbroic intrusions within the Xigaze ophiolite (Tibet): New insights into the origin of ophiolite diversity. *Contributions to Mineralogy and Petrology*, *173*, 91. https://doi.org/10.1016/j.chemgeo.2016.09.015

Liu, T., Wu, F.-Y., Zhang, L.-L., Zhai, Q.-G., Liu, C.-Z., Ji, W.-B., et al. (2016). Zircon U-Pb geochronological constraints on rapid exhumation of the mantle peridotite of the Xigaze ophiolite, southern Tibet. *Chemical Geology*, *173*(11), 1–21. https://doi.org/10.1007/s00410-018-1518-6

Lutz, R., Franke, D., Berglar, K., Heyde, I., Schreckenberger, B., Klitzke, P., & Geissler, W. H. (2018). Evidence for mantle exhumation since the early evolution of the slow-spreading Gakkel ridge, Arctic Ocean. *Journal of Geodynamics*, *118*, 154–165. https://doi.org/10.1016/j.jog.2018.01.014

Maffione, M., van Hinsbergen, D. J. J., Koornneef, L. M. T., Guilmette, C., Hodges, K., Borneman, N., et al. (2015). Forearc hyperextension dismembered the south Tibetan ophiolites. *Geology*, *43*, 475–478. https://doi.org/10.1130/g36472.1

Manatschal, G., & Müntener, O. (2009). A type sequence across an ancient magma-poor ocean–continent transition: The example of the western Alpine Tethys ophiolites. *Tectonophysics*, *473*, 4–19. https://doi.org/10.1016/j.tecto.2008.07.021

McCarthy, A., Chelle-Michou, C., Müntener, O., Arculus, R., & Blundy, J. (2018). Subduction initiation without magmatism: The case of the missing Alpine magmatic arc. *Geology*. https://doi.org/10.1130/G36340.1

McCarthy, A., & Müntener, O. (2015). Ancient depletion and mantle heterogeneity: Revisiting the Permian-Jurassic paradox of Alpine peridotites. *Geology*, *43*, 255–258. https://doi.org/10.1130/G45366.1

Müntener, O., Hermann, J., & Trommsdorff, V. (2000). Cooling history and exhumation of lower-crustal granulite and upper mantle (Malenco, Eastern Central Alps). *Journal of Petrology*, *41*, 175–200.

Nicolas, A., Girardeau, J., Marcoux, J., Dupre, B., Wang, X. B., Cao, Y. G., et al. (1981). The Xigaze Ophiolite (Tibet): A peculiar oceanic lithosphere. *Nature*, *294*, 414–417. https://doi.org/10.1038/294414a0

Park, J., & Rye, D. M. (2019). Broader impacts of the metasomatic underplating hypothesis. *Geochemistry, Geophysics, Geosystems*, *20*, 4810–4829. https://doi.org/10.1029/2019GC008493

Peacock, S. A. (1990). Fluid processes in subduction zones. *Science*, *248*(4953), 329–337. https://doi.org/10.1126/science.248.4953.329

Ramos, V. A., & Folguera, A. (2009). Andean flat-slab subduction through time. *Geological Society - Special Publications*, *327*, 31–54. https://doi.org/10.1144/SP327.3

Ruh, J. B., Le Pourhiet, L., Agard, P., Burov, E., & Gerya, T. (2015). Tectonic slicing of subducting oceanic crust along plate interfaces: Numerical modeling. *Geochemistry, Geophysics, Geosystems*, *16*, 3505–3531. https://doi.org/10.1002/2015GC005998

Schaltegger, U., Desmurs, L., Manatschal, G., Müntener, O., Meier, M., Frank, M., & Bernoulli, D. (2002). The transition from rifting to sea-floor spreading within a magma-poor rifted margin: Field and isotopic constraints. *Terra Nova*, *14*, 156–162. https://doi.org/10.1046/j.1365-3121.2002.00406.x

Schmidt, M. W., & Poli, S. (1998). Experimentally based water budgets for dehydrating slabs and consequences for arc magma generation. *Earth and Planetary Science Letters*, *163*, 361–379. https://doi.org/10.1016/S0012-821X(98)00142-3

Schwartz, S., Allemand, P., & Guillot, S. (2001). Numerical model of the effect of serpentinites on the exhumation of eclogitic rocks: Insights from the Monviso ophiolitic massif (Western Alps). *Tectonophysics*, *342*, 193–206.

Sisson, T., & Bronto, S. (1998). Evidence for pressure-release melting beneath magmatic arcs from basalt at Galunggung, Indonesia. *Nature*, *391*, 883–886.

Sobolev, S. V., & Brown, M. (2019). Surface erosion events controlled the evolution of plate tectonics on Earth. *Nature*, *570*, 52–57.

van Hunen, J., van den Berg, A. P., & Vlaar, N. J. (2004). Various mechanisms to induce present-day shallow flat subduction and implications for the younger Earth: A numerical parameter study. *Physics of the Earth and Planetary Interiors*, *146*, 179–194.

Vogt, K., & Gerya, T. (2014). Deep plate serpentinization triggers skinning of subducting slabs. *Geology*, *42*, 723–726. https://doi.org/10.1130/G35565.1

Wallace, P. J. (2005). Volatiles in subduction zone magmas: Concentrations and fluxes based on melt inclusion and volcanic gas data. *Journal of Volcanology and Geothermal Research*, *140*, 217–240.

Xiong, Q., Griffin, W. L., Zheng, J.-P., O'Reilly, S. Y., Pearson, N. J., Xu, B., & Belousova, E. A. (2016). Southward trench migration at~ 130–120 Ma caused accretion of the Neo-Tethyan forearc lithosphere in Tibetan ophiolites. *Earth and Planetary Science Letters*, *438*, 57–65. https://doi.org/10.1016/j.epsl.2016.01.014

Yang, J., & Faccenda, M. (2020). Intraplate volcanism originating from upwelling hydrous mantle transition zone. *Nature*, *579*(7797), 88–91. https://doi.org/10.1038/s41586-020-2045-y

Yang, J., Zhao, L., Kaus, B. J., Lu, G., Wang, K., & Zhu, R. (2018). Slab-triggered wet upwellings produce large volumes of melt: Insights into the destruction of the North China Craton. *Tectonophysics*, *746*, 266–279. https://doi.org/10.1016/j.tecto.2017.04.009

Zhang, C., Liu, C.-Z., Xu, Y., Ji, W.-B., Wang, J.-M., Wu, F.-Y., et al. (2019). Subduction re-initiation at dying ridge of Neo-Tethys: Insights from mafic and metamafic rocks in Lhaze ophiolitic mélange, Yarlung-Tsangbo suture zone. *Earth and Planetary Science Letters*, *523*, 115,707. https://doi.org/10.1016/j.epsl.2019.07.009

Zheng, Y., Chen, R., Xu, Z., & Zhang, S. (2016). The transport of water in subduction zones. *Science China Earth Sciences*, *59*, 651–682. https://doi.org/10.1007/s11430-015-5258-4